

Isovector axial and pseudoscalar form factors from twisted mass lattice QCD at the physical point

Constantia Alexandrou,^{a,b} Simone Bacchio,^b Martha Constantinou,^c Jacob Finkenrath,^d Roberto Frezzotti,^e Bartosz Kostrzewa,^f Giannis Koutsou,^{b,*} Gregoris Spanoudes^a and Carsten Urbach^f

^aDepartment of Physics, University of Cyprus

^bComputation-based Science and Technology Research Center, The Cyprus Institute

^cDepartment of Physics, Temple University, Philadelphia

^dDepartment of Theoretical Physics, European Organization for Nuclear Research, CERN

^eDipartimento di Fisica and INFN, Università di Roma "Tor Vergata", Rome

^fHISKP (Theory), Rheinische Friedrich-Wilhelms-Universität Bonn

E-mail: g.koutsou@cyi.ac.cy

We present the isovector axial, induced pseudoscalar, and pseudoscalar form factors of the nucleon using three twisted-mass fermion ensembles with degenerate up- and down-, strange-, and charm-quarks with masses tuned to their physical values (physical point). The three ensembles have lattice spacing $a=0.08, 0.068$, and 0.057 fm and approximately equal physical volume allowing for the continuum limit to be taken at the physical point. Excited-state contributions to the matrix elements are evaluated using several sink-source separations from 0.5 fm to 1.5 fm and multistate fits. We check the partially conserved axial-vector current (PCAC) hypothesis and the pion pole dominance (PPD) and show that in the continuum limit both relations are satisfied. We provide results at the continuum limit for the isovector nucleon axial charge, axial radius, pion-nucleon coupling constant, and for the induced pseudoscalar form factor at the muon capture point.

The 41st International Symposium on Lattice Field Theory (LATTICE2024)
28 July - 3 August 2024
Liverpool, UK

*Speaker

1. Introduction

The nucleon axial form factors are fundamental quantities that characterize the nucleon's response to weak interactions and play a crucial role in neutrino scattering experiments. They are particularly relevant for current and upcoming neutrino experiments such as NO ν A, MINER ν A, and DUNE. At Fermi Lab, the MINER ν A experiment has recently provided new measurements of neutrino interactions [1]. While the axial charge g_A is well determined from neutron beta decay experiments [2–5], the momentum dependence of the axial form factor $G_A(Q^2)$ and the induced pseudoscalar form factor $G_P(Q^2)$ are less well constrained by experiment.

Lattice QCD provides a first-principles approach to computing these quantities directly from the QCD Lagrangian. Recent progress has enabled simulations at physical quark masses, eliminating the need for chiral extrapolation which can introduce uncontrolled systematic uncertainties. Early lattice studies were limited to the quenched approximation [6, 7] or heavier than physical pion masses [8]. In this work, we present the first calculation to use solely simulations at physical pion mass to take the continuum limit, using three ensembles generated with twisted mass fermions [9]. The ensembles span lattice spacings from 0.08 fm to 0.057 fm, enabling a controlled continuum extrapolation of all quantities. We perform a thorough analysis of excited-state contributions and examine important relations such as the partially conserved axial-vector current (PCAC) and pion pole dominance (PPD).

2. Axial and pseudo-scalar form factors

The nucleon matrix element of the isovector axial-vector current $A_\mu = \bar{u}\gamma_\mu\gamma_5u - \bar{d}\gamma_\mu\gamma_5d$ can be decomposed in terms of two form factors,

$$\langle N(p', s') | A_\mu | N(p, s) \rangle = \bar{u}_N(p', s') \left[\gamma_\mu G_A(Q^2) - \frac{Q_\mu}{2m_N} G_P(Q^2) \right] \gamma_5 u_N(p, s), \quad (1)$$

where $G_A(Q^2)$ is the axial and $G_P(Q^2)$ the induced pseudoscalar form factor. Here $Q^2 = -q^2$ with $q = p' - p$ the momentum transfer and m_N the nucleon mass. The axial form factor at zero momentum transfer gives the axial charge, $g_A \equiv G_A(0)$, while its slope determines the axial radius,

$$\langle r_A^2 \rangle = -\frac{6}{g_A} \frac{\partial G_A(Q^2)}{\partial Q^2} \Big|_{Q^2 \rightarrow 0}. \quad (2)$$

The nucleon matrix element of the pseudoscalar current $P = \bar{u}\gamma_5u - \bar{d}\gamma_5d$ defines the pseudoscalar form factor,

$$\langle N(p', s') | P | N(p, s) \rangle = G_5(Q^2) \bar{u}_N(p', s') \gamma_5 u_N(p, s). \quad (3)$$

These form factors are related through the partially conserved axial-vector current (PCAC) relation,

$$G_A(Q^2) - \frac{Q^2}{4m_N^2} G_P(Q^2) = \frac{m_q}{m_N} G_5(Q^2), \quad (4)$$

where m_q is the light quark mass. Near the pion pole, assuming pion pole dominance (PPD), the induced pseudoscalar form factor can be expressed as,

$$G_P(Q^2) = \frac{4m_N^2}{Q^2 + m_\pi^2} G_A(Q^2), \quad (5)$$

where m_π is the pion mass. Both PCAC and PPD relations will be examined in the continuum limit of our lattice calculation. We also compute the induced pseudoscalar coupling determined at the muon capture point,

$$g_P^* = \frac{m_\mu}{2m_N} G_P(0.88 m_\mu^2), \quad (6)$$

where m_μ is the muon mass, as well as the pion-nucleon coupling constant $g_{\pi NN}$ defined through the pseudoscalar form factor at the pion pole.

3. Lattice setup and statistics

We describe the ensembles used in this work and detail the statistics for computing correlation functions.

We use three $N_f=2+1+1$ twisted mass fermion ensembles at the physical point with lattice spacings spanning from 0.08 fm to 0.057 fm. The parameters of these ensembles are given in Table 1. The bare light quark mass parameter μ_l is tuned to reproduce the isosymmetric pion mass $m_\pi = 135$ MeV, while the heavy quark parameters μ_s and μ_c are tuned via the ratio of D-meson mass to decay constant and the ratio of the strange to charm quark mass [10, 11].

Table 1: Parameters of the $N_f=2+1+1$ ensembles analyzed in this work. We give the lattice volume, $\beta = 6/g^2$ with g the bare coupling constant, the lattice spacing a , the number of gauge configurations N_{conf} , the pion mass m_π , and $m_\pi L$. Lattice spacings and pion masses are taken from Ref. [12].

Ensemble	V/a^4	β	a [fm]	N_{conf}	m_π [MeV]	$m_\pi L$
cB211.072.64	$64^3 \times 128$	1.778	0.07957(13)	750	140.2(2)	3.62
cC211.060.80	$80^3 \times 160$	1.836	0.06821(13)	400	136.7(2)	3.78
cD211.054.96	$96^3 \times 192$	1.900	0.05692(12)	500	140.8(2)	3.90

For each ensemble, we compute two- and three-point correlation functions using multiple source positions per gauge configuration. For two-point functions, we use 477, 650, and 480 source positions for the three ensembles respectively. For three-point functions, we employ seven to ten different sink-source time separations ranging from approximately 0.5 fm to 1.5 fm. The number of source positions per configuration is increased with the sink-source separation to maintain approximately constant statistical errors, ranging from $\mathcal{O}(1)$ for the shortest separation to $\mathcal{O}(100)$ for the largest [9].

We neglect disconnected quark loop contributions in the present work since in the twisted mass formulation these contributions to isovector matrix elements are of order a^2 and thus vanish in the continuum limit [13].

The matrix elements are renormalized non-perturbatively using methods based on Ward identities, which are fully non-perturbative and require no gauge fixing [12]. This approach provides much more accurate results on the renormalization constants compared to the standard RI' scheme.

4. Extraction of Form Factors

The nucleon matrix elements are determined from two- and three-point correlation functions. The spectral decomposition of the two-point function is given by

$$C(\Gamma_0, \vec{p}, t_s) = \sum_i^{N_{st}-1} c_i(\vec{p}) e^{-E_i(\vec{p})t_s} \quad (7)$$

and the three-point function by

$$C_\mu(\Gamma_k, \vec{q}, t_s, t_{\text{ins}}) = \sum_{i,j}^{N_{st}-1} \mathcal{A}_\mu^{i,j}(\Gamma_k, \vec{q}) e^{-E_i(\vec{0})(t_s-t_{\text{ins}})-E_j(\vec{q})t_{\text{ins}}}, \quad (8)$$

with t_s the sink time and t_{ins} the current insertion time. The coefficients $c_i(\vec{p})$ are overlap terms of the interpolating operator with the i -th state while $\mathcal{A}_\mu^{i,j}$ contain the matrix elements between states i and j . The desired ground-state matrix element is obtained by $\frac{\mathcal{A}_\mu^{0,0}(\Gamma_k, \vec{q})}{\sqrt{c_0(\vec{0})c_0(\vec{q})}}$. The coefficients $c_i(\vec{p})$ and $\mathcal{A}_\mu^{i,j}$ are determined by simultaneous fits to two- and three-point functions at multiple t_s . The sums of Eqs. (7) and (8) are truncated at either $N_{st} = 2$ (two-state fits) or $N_{st} = 3$ (three-state fits). For the lowest non-zero momentum transfer, we perform combined fits to matrix elements of the axial current including both spatial and temporal components, to better constrain the excited state energies in the fits. For each fit we vary i) the minimum value of t_s included in the fit range of the two-point function ($t_{2\text{pt}, \text{min}}$), ii) the minimum value of t_s included in the fit range of the three-point function ($t_{3\text{pt}, \text{min}}$), iii) the number of insertion time slices kept near the source ($t_{\text{ins}, 0}$) and sink ($t_{\text{ins}, s}$), and iv) for three-state fits, we include either only the terms $\mathcal{A}_\mu^{0,0}, \mathcal{A}_\mu^{1,0}, \mathcal{A}_\mu^{0,1}, \mathcal{A}_\mu^{1,1}, \mathcal{A}_\mu^{2,0}, \mathcal{A}_\mu^{0,2}$ ($N_O = 6$), or all terms of the three-state fit, i.e. including $\mathcal{A}_\mu^{2,1}, \mathcal{A}_\mu^{1,2}, \mathcal{A}_\mu^{2,2}$ ($N_O = 9$).

The results from different fit ranges are combined using the Akaike Information Criterion (AIC). To each fit i we assign a weight

$$\log(w_i) = -\frac{\chi_i^2}{2} + N_{\text{dof}, i}, \quad (9)$$

where $N_{\text{dof}} = N_{\text{data}} - N_{\text{params}}$ is the number of degrees of freedom [14, 15]. The model averaged value of an observable O is then given by $\langle O \rangle = \sum_i \bar{O}_i p_i$ and its error squared by $\sum_i (\sigma_i^2 + \bar{O}_i^2) p_i - \langle O \rangle^2$, where $p_i = w_i / \sum_j w_j$ and \bar{O}_i and σ_i are the central value and error from fit i .

In Fig. 1 we provide an example analysis for the intermediate lattice spacing, with results for all ensembles given in Ref. [9]. For visualization purposes, we construct the ratio,

$$R'_\mu(\Gamma_k; \vec{q}; t_s, t_{\text{ins}}) = \frac{C_\mu(\Gamma_k, \vec{q}; t_s, t_{\text{ins}})}{\sqrt{C(\Gamma_0, \vec{0}; t_s)C(\Gamma_0, \vec{q}; t_s)}}, \quad (10)$$

which at large time-separations $t_s - t_{\text{ins}} \gg$ and $t_s \gg$ yields the ground-state matrix element. Both two- and three-state fits yield consistent results, with the most probable fits having probabilities between 10% and 50%.

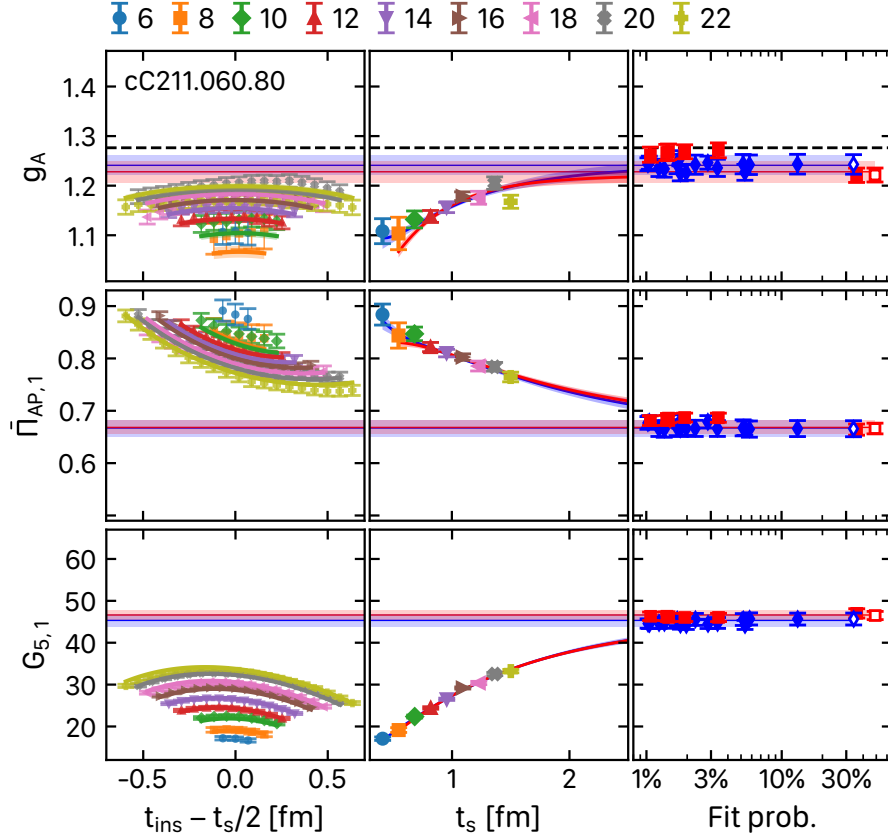


Figure 1: The ratio of Eq. (10) for the ensemble cC211.060.80 and for three cases, namely that yielding g_A (top), that yielding a linear combination of the axial and induced pseudoscalar form factor at the first non-zero momentum transfer (middle) and that yielding the pseudoscalar form factor at the first non-zero momentum transfer (bottom). In the left column we plot the ratio versus the insertion time, in the middle we plot for $t_{\text{ins}} = t_s/2$ and in the right column we show the asymptotic value of the two- (blue) or three- (red) state fits versus the fit probability. In the left and middle columns, the curves correspond to the fit results which have the largest probability.

5. Results for axial and pseudoscalar form factors

We analyze the Q^2 -dependence of the axial form factor using both dipole and z-expansion parameterizations. The dipole Ansatz is given by $G(Q^2) = \frac{g}{(1 + \frac{Q^2}{m^2})^2}$, with the axial radius given by $\langle r^2 \rangle = 12/m^2$.

The z-expansion is given as $G(Q^2) = \sum_{k=0}^{k_{\text{max}}} a_k z^k(Q^2)$, where $z(Q^2) = \frac{\sqrt{t_{\text{cut}} + Q^2} - \sqrt{t_{\text{cut}} + t_0}}{\sqrt{t_{\text{cut}} + Q^2} + \sqrt{t_{\text{cut}} + t_0}}$, with $t_{\text{cut}} = (3m_\pi)^2$ and $t_0 = 0$. The coefficients a_k are constrained using Gaussian priors centered at zero with width that falls like $1/k$ to ensure smooth convergence at large Q^2 .

For both parameterizations, we account for cut-off effects by allowing a linear a^2 dependence in the parameters. The analysis is performed in two ways, namely fitting the Q^2 -dependence for each ensemble separately followed by continuum extrapolation of the parameters (two-step), or fitting all ensembles simultaneously (one-step). Both approaches yield consistent results. We find

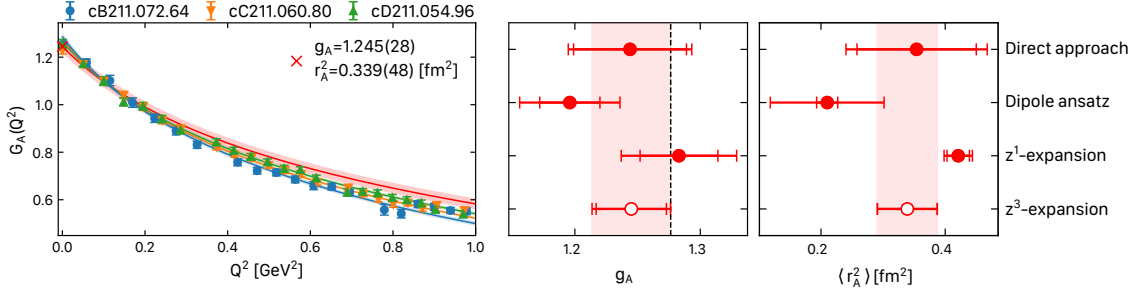


Figure 2: Left: The axial form factor $G_A(Q^2)$ determined from two-state fits (red band) with systematic uncertainty from the difference with three-state fits (yellow band). Results at finite lattice spacing shown in blue, orange and green bands. Right: Results for the axial charge g_A and radius $\langle r_A^2 \rangle$ obtained using different analysis approaches.

convergence of the z-expansion at $k_{\max} = 3$ and verify stability with respect to the prior width and maximum Q^2 included in the fits. The analysis is performed separately for the matrix elements extracted using two- and three-state fits. The two-state fits allow analysis up to $Q^2 = 1 \text{ GeV}^2$, while three-state fits become unstable beyond $Q^2 \simeq 0.5 \text{ GeV}^2$. The results from both analyses are consistent within the range where three-state fits are stable. The resulting form axial factor using a two-state fit analysis is shown in the left panel of Fig. 2.

Our final results use the z-expansion fits to the two-state data as central values, with a systematic error taken as the difference between the central values when using two- or three-state fits. The values for g_A and $\langle r_A^2 \rangle$ using this approach are in the right panel of Fig. 2, where the direct extraction is also shown, i.e. by computing the radius from $Q^2 = 0$ and the lowest non-zero Q^2 . The consistency among these different approaches, particularly between the direct approach and z-expansion which uses data at all Q^2 , demonstrates the robustness of our analysis.

The induced pseudoscalar $G_P(Q^2)$ and pseudoscalar $G_5(Q^2)$ form factors exhibit a pion pole at $Q^2 = -m_\pi^2$. For $G_5(Q^2)$ we analyze the scaled quantity, $\tilde{G}_5(Q^2) = \frac{4m_N}{m_\pi^2} m_q G_5(Q^2)$, where the combination $m_q G_5(Q^2)$ is scale-independent and renormalizes with Z_S/Z_P . The scaling by $1/m_\pi^2$ accounts for slight variations in the simulated pion masses, while m_N makes the combination dimensionless. We perform a combined fit of both form factors using a third-order z-expansion after factoring out the pion pole. Since the pion pole dominance relation is satisfied at the continuum limit, we enforce the value of the pion-nucleon coupling constant $g_{\pi NN}$ extracted from both form factors to be the same. The resulting form factors are shown in Fig. 3, where the inner panels highlight the behavior near the pion pole.

6. PCAC and pion pole dominance

We examine the PCAC and PPD relations by constructing the ratios

$$r_{\text{PCAC}}(Q^2) = \frac{\frac{m_q}{m_N} G_5(Q^2) + \frac{Q^2}{4m_N^2} G_P(Q^2)}{G_A(Q^2)} \quad \text{and} \quad r_{\text{PPD}}(Q^2) = \frac{m_\pi^2 + Q^2}{4m_N^2} \frac{G_P(Q^2)}{G_A(Q^2)}. \quad (11)$$

The PCAC relation requires $r_{\text{PCAC}} = 1$ for all Q^2 , while PPD predicts $r_{\text{PPD}} = 1$ near the pion pole.

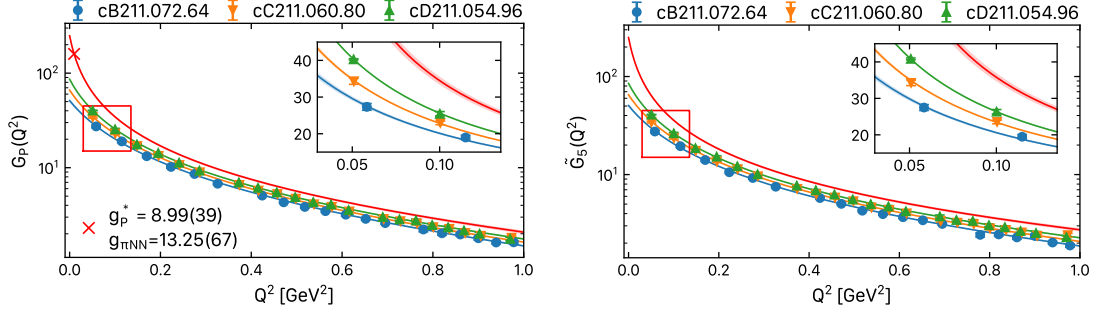


Figure 3: Left: The induced pseudoscalar form factor $G_P(Q^2)$ and right: the pseudoscalar form factor $\tilde{G}_5(Q^2)$ at finite lattice spacing (blue, orange and green bands) and in the continuum limit (red band). Results are obtained using two-state fits and z-expansion of order 3. The inner panels show the region near the pion pole enlarged.

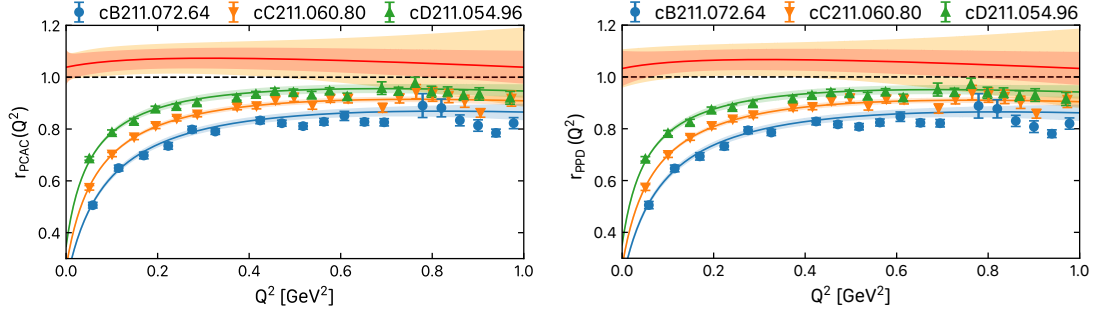


Figure 4: Left: Ratio testing the PCAC relation. Right: Ratio testing pion pole dominance. Results at finite lattice spacing shown in blue, orange and green bands and in the continuum limit with red band. The yellow band includes systematic uncertainties from excited states.

In the twisted mass formulation at finite lattice spacing, we observe sizable cut-off effects in both ratios. These arise from $\mathcal{O}(a^2)$ effects in the pion mass that enter through the pion pole in $G_P(Q^2)$ and $G_5(Q^2)$. The pion pole mass obtained using valence Osterwalder-Seiler quarks in the mixed action formulation shows significant cut-off effects, much larger than the mass splitting between the unitary charged and neutral pion. However, as shown in Fig. 4, both relations are restored in the continuum limit where the pion pole mass agrees with the physical pion mass. Thus, at the continuum limit, our results reproduce these fundamental relations that follow from chiral symmetry.

7. Summary

We have presented a lattice QCD calculation of the nucleon isovector axial, induced pseudoscalar, and pseudoscalar form factors using three ensembles simulated with quark masses that reproduce the physical pion mass. The use of ensembles simulated solely at the physical point eliminates systematic uncertainties from chiral extrapolation. The three ensembles span lattice spacings from 0.08 fm to 0.057 fm with approximately equal physical volumes, enabling a con-

trolled continuum extrapolation. Our analysis shows that both the PCAC relation and pion pole dominance are satisfied in the continuum limit, despite sizable cut-off effects at finite lattice spacing arising from the pion pole in the twisted mass formulation.

Through a careful analysis of excited states and model averaging of multiple fit variations, we obtain, in the continuum limit, the axial charge (g_A), axial radius ($\langle r_A^2 \rangle$), induced pseudoscalar coupling (g_P^*), and pion-nucleon coupling constant ($g_{\pi NN}$),

$$\begin{aligned} g_A &= 1.245(28)(14), & \langle r_A^2 \rangle &= 0.339(48)(06) \text{ fm}^2, \\ g_P^* &= 8.99(39)(49), \text{ and } & g_{\pi NN} &= 13.25(67)(69), \end{aligned} \quad (12)$$

where the first error is statistical from the model average of two-state fits and the second is systematic from excited states. The analysis presented here will be further improved by including a fourth ensemble with lattice spacing $a = 0.049$ fm and approximately same physical volume as the three ensembles used here, with lattice volume $112^3 \times 224$. This will provide an additional point in the continuum extrapolation at an even finer lattice spacing, helping to further constrain cut-off effects and improve the precision of our final results. The analysis of this ensemble is ongoing, with first results for charges presented in Ref. [16].

Acknowledgments

C.A., G.K., and G.S. acknowledge partial support by the projects 3D-nucleon, NiceQuarks, and “Lattice Studies of Strongly Coupled Gauge Theories: Renormalization and Phase Transition” (EXCELLENCE/0421/0043, EXCELLENCE/0421/0195, and EXCELLENCE/0421/0025) co-financed by the European Regional Development Fund and the Republic of Cyprus through the Research and Innovation Foundation as well as AQTIVATE that received funding from the European Union’s research and innovation program under the Marie Skłodowska-Curie Doctoral Networks action, Grant Agreement No 101072344. C.A acknowledges support by the University of Cyprus projects “Nucleon-GPDs” and “PDFs-LQCD”. S.B. and J.F. are supported by the Inno4scale project, which received funding from the European High-Performance Computing Joint Undertaking (JU) under Grant Agreement No. 101118139. J.F. also acknowledges support from the DFG research unit FOR5269 “Future methods for studying confined gluons in QCD” and the Next Generation Triggers project. M.C. acknowledges financial support from the U.S. Department of Energy, Office of Nuclear Physics under Grant No. DE-SC0020405, and the Grant No. DE-SC0025218. R.F. is supported by the Italian Ministry of University and Research (MUR) under the grant PNRR-M4C2-I1.1-PRIN 2022-PE2 Non-perturbative aspects of fundamental interactions, in the Standard Model and beyond F53D23001480006 funded by E.U.- NextGenerationEU. This work was supported by the Deutsche Forschungsgemeinschaft (DFG, German Research Foundation) as part of the CRC 1639 NuMeriQS – project no. 511713970. This work was supported by grants from the Swiss National Supercomputing Centre (CSCS) under projects with ids s702 and s1174. The authors gratefully acknowledge the Gauss Centre for Supercomputing e.V. (www.gauss-centre.eu) for funding this project by providing computing time through the John von Neumann Institute for Computing (NIC) on the GCS Supercomputer JUWELS-Booster at Jülich Supercomputing Centre (JSC). The authors also acknowledge the Texas Advanced Computing Center (TACC) at The University of Texas at Austin for providing HPC resources that have contributed to the research results.

References

- [1] MINERvA collaboration, T. Cai et al., *Measurement of the axial vector form factor from antineutrino–proton scattering*, *Nature* **614** (2023) 48.
- [2] UCNA collaboration, M. A. P. Brown et al., *New result for the neutron β -asymmetry parameter A_0 from UCNA*, *Phys. Rev. C* **97** (2018) 035505 [[1712.00884](#)].
- [3] G. Darius et al., *Measurement of the Electron-Antineutrino Angular Correlation in Neutron β Decay*, *Phys. Rev. Lett.* **119** (2017) 042502.
- [4] UCNA collaboration, M. P. Mendenhall et al., *Precision measurement of the neutron β -decay asymmetry*, *Phys. Rev. C* **87** (2013) 032501 [[1210.7048](#)].
- [5] D. Mund, B. Maerkisch, M. Deissenroth, J. Krempel, M. Schumann et al., *Determination of the Weak Axial Vector Coupling from a Measurement of the Beta-Asymmetry Parameter A in Neutron Beta Decay*, *Phys. Rev. Lett.* **110** (2013) 172502 [[1204.0013](#)].
- [6] K.-F. Liu, J.-M. Wu, S.-J. Dong and W. Wilcox, *Lattice calculation of nucleon axial form-factors*, *Nucl. Phys. B Proc. Suppl.* **20** (1991) 467.
- [7] K. F. Liu, S. J. Dong, T. Draper, J. M. Wu and W. Wilcox, *Nucleon axial form-factor from lattice QCD*, *Phys. Rev. D* **49** (1994) 4755 [[hep-lat/9305025](#)].
- [8] C. Alexandrou, G. Koutsou, T. Leontiou, J. W. Negele and A. Tsapalis, *Axial Nucleon and Nucleon to Delta form factors and the Goldberger-Treiman Relations from Lattice QCD*, *Phys. Rev. D* **76** (2007) 094511 [[0706.3011](#)], [Erratum: *Phys. Rev. D* **80** (2009) 099901].
- [9] EXTENDED TWISTED MASS collaboration, C. Alexandrou, S. Bacchio, M. Constantinou, J. Finkenrath, R. Frezzotti et al., *Nucleon axial and pseudoscalar form factors using twisted-mass fermion ensembles at the physical point*, *Phys. Rev. D* **109** (2024) 034503 [[2309.05774](#)].
- [10] J. Finkenrath et al., *Twisted mass gauge ensembles at physical values of the light, strange and charm quark masses*, *PoS LATTICE2021* (2022) 284 [[2201.02551](#)].
- [11] C. Alexandrou et al., *Simulating twisted mass fermions at physical light, strange and charm quark masses*, *Phys. Rev. D* **98** (2018) 054518 [[1807.00495](#)].
- [12] EXTENDED TWISTED MASS collaboration, C. Alexandrou et al., *Lattice calculation of the short and intermediate time-distance hadronic vacuum polarization contributions to the muon magnetic moment using twisted-mass fermions*, *Phys. Rev. D* **107** (2023) 074506 [[2206.15084](#)].
- [13] R. Frezzotti and G. C. Rossi, *Chirally improving Wilson fermions. I. $O(a)$ improvement*, *JHEP* **08** (2004) 007 [[hep-lat/0306014](#)].
- [14] W. I. Jay and E. T. Neil, *Bayesian model averaging for analysis of lattice field theory results*, *Phys. Rev. D* **103** (2021) 114502 [[2008.01069](#)].

- [15] E. T. Neil and J. W. Sitison, *Improved information criteria for Bayesian model averaging in lattice field theory*, *Phys. Rev. D* **109** (2024) 014510 [[2208.14983](#)].
- [16] C. Alexandrou, S. Bacchio, C. Iona, G. Koutsou, Y. Li et al., *Nucleon axial, tensor, and scalar charges and σ -terms in lattice QCD*, *PoS LATTICE2024* (2025) 316.